From weak antilocalization to Kondo scattering in a magnetic complex oxide interface

Xinxin Cai,[1] Jin Yue,[2] Peng Xu,[2] Bharat Jalan,[2] and Vlad S. Pribiag[1,*]

[1]*School of Physics and Astronomy, University of Minnesota, Minneapolis, Minnesota 55455, USA*

[2]*Department of Chemical Engineering and Materials Science, University of Minnesota, Minneapolis, Minnesota 55455, USA*

(Received 15 October 2020; revised 9 February 2021; accepted 5 March 2021; published 22 March 2021)

Quantum corrections to electrical resistance can serve as sensitive probes of the magnetic landscape of a material. For example, interference between time-reversed electron paths gives rise to weak localization effects, which can provide information about the coupling between spins and orbital motion, while the Kondo effect is sensitive to the presence of spin impurities. Here, we use low-temperature magnetotransport measurements to reveal a gradual transition from weak antilocalization (WAL) to Kondo scattering in the quasi-two-dimensional electron gas formed at the interface between $SrTiO_3$ and the Mott insulator $NdTiO_3$. This transition occurs as the thickness of the $NdTiO_3$ layer is increased. Analysis of the Kondo scattering and WAL points to the presence of atomic-scale magnetic impurities coexisting with nanoscale magnetic regions that affect transport via a strong magnetic exchange interaction. This leads to distinct magnetoresistance behaviors that can serve as a sensitive probe of magnetic properties in two dimensions.

DOI: 10.1103/PhysRevB.103.115434

I. INTRODUCTION

Conducting interfaces between $SrTiO_3$ (STO) and other complex oxides are an ideal system for investigating two-dimensional (2D) electron systems in the high-density regime [1–4]. Our experimental system consists of epitaxial layers of $SrTiO_3$ and $NdTiO_3$ (NTO) [4–6], which host a high-density quasi-two-dimensional electron gas coupled to local ferromagnetic or superparamagnetic regions [7,8]. The ferromagnetic order is thought to originate from spatially inhomogeneous canting of the antiferromagnetically aligned spins in NTO [7,9], which is a Mott-Hubbard insulator with a Néel temperature of $\sim$90 K [10,11]. Here, we focus on MBE-grown heterostructures with layer structure STO(8 u.c.)/NTO(x u.c.)/STO(8 u.c.)/(La, Sr)(Al, Ta)O_3 (LSAT)(001) (substrate), where $x = 2$, 4, 10, 20 [Fig. 1(a)]. The top STO layer protects the underlying heterostructure from degradation [6], however, only the bottom NTO-on-STO interface is expected to contribute to transport, as STO-on-NTO interfaces are typically insulating at low temperatures [5,7]. In this system, itinerant electrons, which reside primarily on the STO side of the interface [5], experience the combined effect of k-cubic Rashba spin-orbit coupling (SOC) and a magnetic exchange interaction of several 10's of Tesla due to the local magnetic order [8].

Previous work has focused on the case of thin NTO layers, where an applied parallel field gives rise to a unique type of weak antilocalization (WAL) correction to the conductance under the combined effect of the spin-orbit coupling and the magnetic exchange [8]. Here we report on a striking transition from this regime, where localization effects dominate the magnetotransport response, to a regime of predominant Kondo scattering, as the thickness of the NTO layer is increased. Interestingly, for the thickest NTO layers studied, the Kondo effect coexists with the interfacial exchange interaction, suggesting the presence in close proximity of both atomic-scale spin impurities and larger magnetically ordered regions.

II. EXPERIMENTAL DETAILS

The heterointerfaces are mesa-etched into 10×20 and 10×40 μm^2 Hall-bar devices by a combination of electron beam lithography and dry etching techniques. Figure 1(a) shows a typical device. To achieve Ohmic contacts to the conducting interfaces, the cross sections of the heterostructures are exposed by Ar-ion milling and coated afterwards by Ti/Au electrodes via an angled deposition. The magnetotransport measurements are performed in a 9-T Quantum Design physical property measurement system (PPMS) at temperatures (T) down to 2 K. A rotational sample holder is used for applying magnetic fields at various angles with respect to the sample plane. Four-terminal resistance is measured using standard DC techniques with currents $\leqslant 0.5$ μA. We estimate the electron mobility μ of the samples based on the longitudinal resistance and Hall effect data. The estimated μ values are presented in Fig. 1(b) for a broad range of temperatures.

III. RESULTS AND DISCUSSION

Figure 1(c) shows the sample magnetoresistance (MR) as a function of perpendicular field $B_\perp$ measured at $T = 2$ K. The data for the 2 u.c. sample has the characteristic shape of WAL, with sharp positive MR clearly seen around zero field, and a maximum value at larger field, around $B_\perp = 2$ T. The WAL/WL contribution to the magetoresistance in $B_\perp$ can

*vpribiag@umn.edu

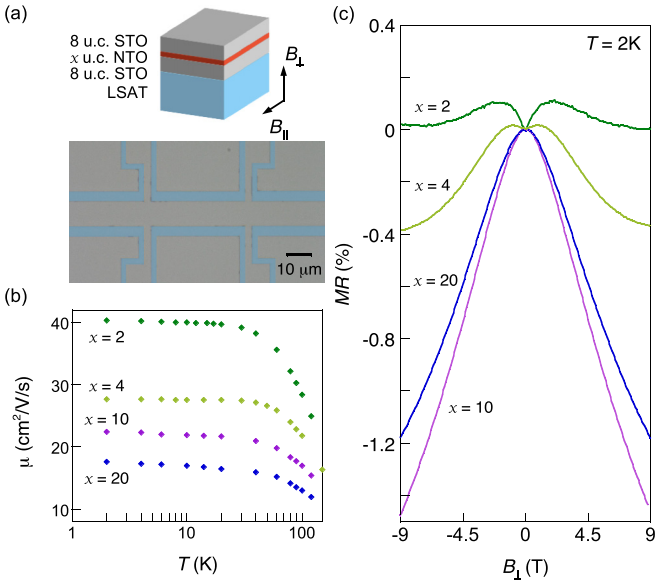

FIG. 1. (a) Top: a schematic of the STO(8 u.c.)/NTO(x u.c.)/STO(8 u.c.)/LSAT(001) heterostructure, where $x = 2, 4, 10, 20$. The directions of applied fields are indicated with respect to the heterointerface. Bottom: false-color optical image of a typical Hall-bar sample prepared on the heterostructure. The etched regions are indicated in blue. (b) The temperature dependence of the Hall mobility μ. (c) Magnetoresistance as a function of the perpendicular magnetic field $B_\perp$ measured at $T = 2$ K. The $x = 2$ data in (b) and (c) are reproduced from Ref. [8] to allow direct comparison with the $x = 4$, 10, and 20 samples.

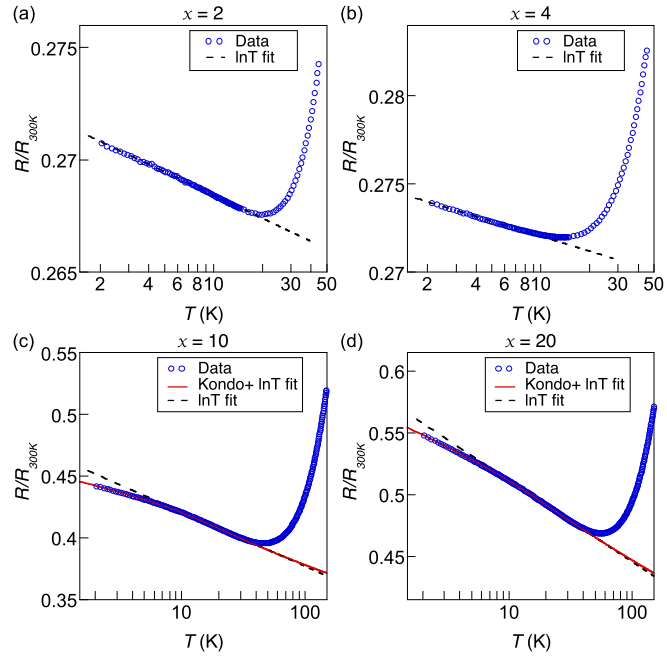

FIG. 2. Sample resistance R (dots) at $B = 0$ as a function of temperature T on a logarithmic scale, normalized to its value at $T = 300$ K, for the STO(8 u.c.)/NTO(x u.c.)/STO(8 u.c.)/LSAT(001) heterostructures, with $x = 2$, 4, 10, and 20, respectively, for (a), (b), (c), and (d). Dashed lines show the low-temperature logarithmic dependencies and solid lines correspond to the theoretical fits using Eqs. (1) and (2). The data in (a) are reproduced from Ref. [8] and rescaled in the same way as (b)–(d) for direct comparison.

be analyzed to extract the dephasing and SOC parameters of the system B_ϕ and B_{so}, respectively [8]. The focus of this work is on the dependence of the MR on the NTO thickness. Figure 1(c) shows four snapshots of this striking evolution. As is shown below, the pronounced negative MR in the thicker samples originates from the interplay between localization and the Kondo effect, with the $x = 4$ sample revealing crossover behavior.

Figure 2 shows the temperature dependence of resistance R, normalized to its value at $T = 300$ K, for devices with four different thicknesses of the NTO layer. An upturn in resistance is observed at low temperatures for all the samples. For samples with 2 or 4 u.c. NTO, the resistance upturn follows a logarithmic dependence on temperature down to 2 K [dashed lines in Figs. 2(a) and 2(b)]. In contrast, as the thickness of the NTO layer is increased to 10 and 20 u.c., the experimental resistance upturn deviates from and lies below the logarithmic dependence for $T <\sim 10$ K [Figs. 2(c) and 2(d)]. Saturation of the logarithmic dependence at low temperatures is characteristic of the Kondo effect, originating from the interplay between the conduction electrons and magnetic impurities.

We find that the R vs T behavior of 10 and 20 u.c. samples at low temperatures can be well described by a simple model, where the Kondo contribution R_K is taken into account, given as

$$R(T) = R_0 - q \ln T + R_K(T). \quad (1)$$

The $\ln T$ term represents the nonsaturating resistance upturn likely due to weak localization (WL) (Appendix B). R_0 includes both a T-independent term from the WAL/WL contribution and the residual resistance due to sample disorder. For the Kondo contribution, we adopt the empirical relation [12,13]

$$R_K(T) = R_K(T = 0)[(T/T_K)^2(2^{1/s} - 1) + 1]^{-s}, \quad (2)$$

which is a universal function of T in units of the Kondo temperature T_K. Here, T_K is defined as the temperature at which the Kondo contribution to the resistance reaches half of its zero-temperature value. The value of s depends on the spin of the impurity (S) and is typically taken to be $s = 0.225$ for $S = \frac{1}{2}$ [12]. Equation (2) is known to work well for a broad range of temperatures, from the logarithmic-dependence dominated region at $T \gg T_K$ to the Fermi-liquid region at $T \ll T_K$. The solid curves in Figs. 2(c) and 2(d) are the fitting results for our data using Eqs. (1) and (2). The extracted values of the fit parameters are listed in Table I. At these low temperatures, the contribution with a power-law temperature dependence due to the electron-phonon interaction almost freezes out [12,14]. For this reason and to minimize

TABLE I. Parameters extracted from the fits to the measured R vs T curves using Eqs. (1) and (2) for a typical 10 and 20 u.c. sample.

x (u.c.)	T_K (K)	$R_K(T = 0)$ (Ω)	R_0 (Ω)	q (Ω)
10	50	60	728	19
20	51	75	1170	46

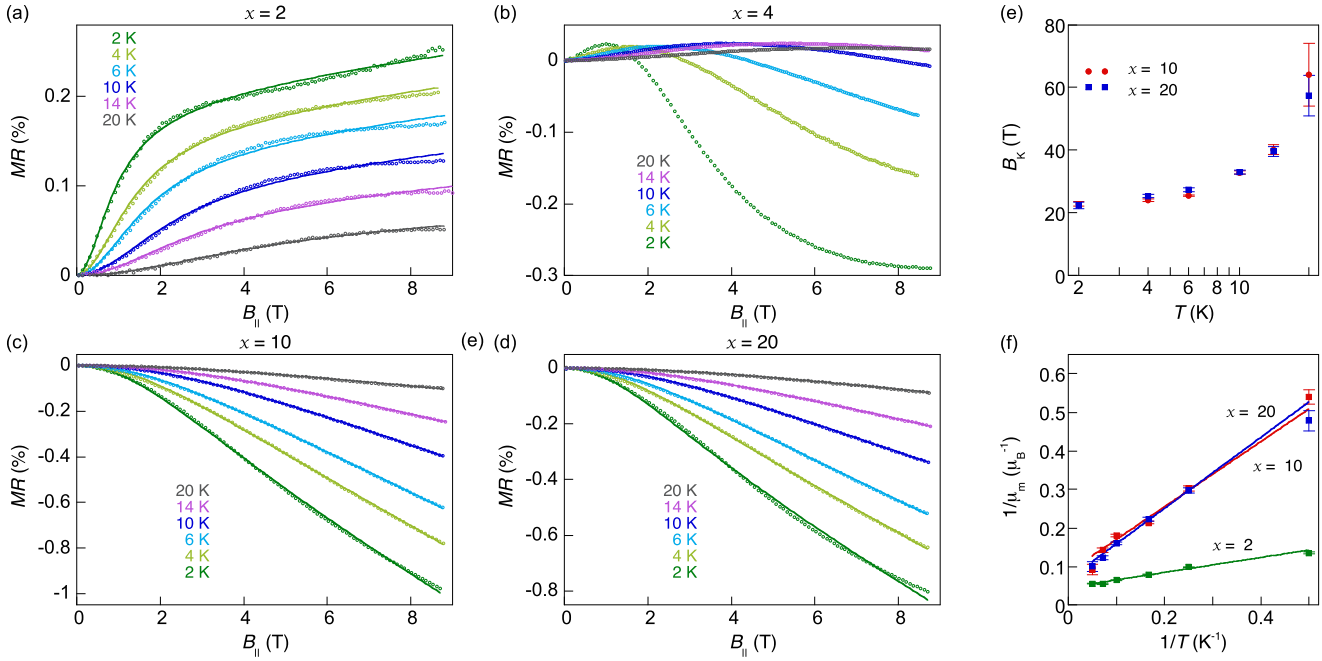

FIG. 3. Magnetoresistance as a function of the parallel field $B_\parallel$ at various temperatures for samples with different NTO thicknesses, $x = 2$ (a), 4 (b), 10 (c), 20 u.c. (d). Experimental data (dots) and theoretical fits (solid lines). (e) The magnetic field scale B_K of the Kondo contribution extracted from the fits in (c) and (d) for the 10 and 20 u.c. samples, respectively. (f) The inverse of the apparent local moment $1/\mu_m$ as function of $1/T$ (dots) and the associated linear fits (solid lines) for the samples in (a), (c), and (d). The vertical bars in (e) and (f) represent the standard errors of the data obtained from the fits. The data on the $x = 2$ sample in (a) and (f) are replotted here based on Ref. [8] for direct comparison.

the number of fit parameters, this term was ignored in our analysis.

The above analysis seems to suggest that both the localization and the Kondo effect contribute to the conductance of the interface in the thicker samples. To distinguish between the contributions, we measure the MR in a magnetic field applied parallel to the sample plane for the low-temperature range. In this case, the orbital effects are expected to be suppressed by the confinement in the z direction due to the two-dimensional (2D) nature of the system. This measurement therefore provides a platform for investigating the magnetic properties of the interfacial system. Figures 3(a)–3(d) show the experimentally measured MR in a parallel magnetic field $[R(B_\parallel) - R(0)]/R(0) \times 100\%$ for samples with different NTO thicknesses. As shown in Fig. 3(a), for a 2 u.c. sample we observe pronounced positive MR for the entire temperature range, with a sharp rise in resistance at low fields and a gradual increase at higher fields. As the NTO thickness increases to 4 u.c., while the low-field regime still features a positive MR, a high-field regime characterized by a negative MR appears for each temperature [Fig. 3(b)]. The negative MR regime is more noticeable at a lower temperature. As the NTO thickness increases further to 10 or 20 u.c., we find that the MR remains negative over the entire field range [Figs. 3(c) and 3(d)].

Previous analysis of the large positive MR observed in 2 u.c. samples revealed the significant roles played by the SOC and local magnetism on the conductance of the interface [8]. It is known that a parallel field can suppress WAL via the Zeeman interaction, resulting in positive MR. The presence of ferromagnetic order in localized regions at the interface gives rise to a substantial magnetic exchange interaction with the conduction electron spins, as compared to the usual case with only the bare applied field. This exchange interaction effectively leads to a large Zeeman splitting and thus affects strongly the sample resistance. These phenomena can be assessed numerically based on localization theories [8]. The Zeeman interaction induces dephasing to the quantum interference in the presence of SOC, which can be described as a correction to the dephasing parameter B_ϕ in the form of [15,16]

$$\Delta_\phi(B_\parallel) = \frac{(g\mu_B B_\parallel)^2}{(4eD)^2 B_{so}}. \tag{3}$$

D is the diffusion coefficient, which can be derived as $D = \pi\hbar^2/(e^2 R_s(0) m^*)$ [8]. The interference-induced magnetoresistance in a parallel magnetic field is thus given by

$$\frac{R_s(B_\parallel) - R_s(0)}{R_s(0)^2} = \frac{\sigma_0}{2} \ln\left[1 + \frac{\Delta_\phi(B_\parallel)}{B_\phi}\right], \tag{4}$$

where R_s represents the sheet resistance and $\sigma_0 = e^2/\pi h$. The exchange interaction from local magnetic regions can be represented by an effective exchange field B^E, which couples to conduction electron spins, and enters the formulas via the Zeeman term [17]. As a result, the applied field $B_\parallel$ in Eqs. (3) and (4) is replaced by a total effective field in the plane $B_\parallel^t = B_\parallel + B_\parallel^E$. In a superparamagnetic system, the fluctuating moments μ_m of local magnetic regions tend to align along the applied magnetic field, leading to a net magnetization [18]. In this case, the applied field dependence of the exchange field is given by the Langevin function $L(x)$ at temperatures above the blocking temperatures, yielding $B_\parallel^E(B_\parallel) = \lambda\mu_0 M_s L(\mu_m B_\parallel/k_B T)$, where λ is the coefficient characteriz-

ing the effective exchange interaction between electrons and the local moments, μ_m is the moment of a single magnetic region, and M_s is the saturation magnetization.

Using $\lambda\mu_0 M_s$ and μ_m as two variables, the MR data for the 2 u.c. sample are well reproduced by the fits incorporating the Langevin function into Eqs. (3) and (4) as described above. The fits are shown as solid lines in Fig. 3(a) for various temperatures. Here, the values of B_{so} and B_ϕ are obtained from the fitting of the MR vs $B_\perp$ data for the same sample using standard WAL formulas (see Appendix B). Equation (3) depends on the product of the g factor and the effective mass m^*. The slope of $\sqrt{\Delta_\phi}$ vs $B_\parallel$ at 2 K for large $B_\parallel$, where $B_\parallel^E$ shows saturating behavior, yields $gm^*/m_e \sim 1.5$. We note the above analysis is limited to the condition $\Delta_\phi < B_{so}$, according to the localization theory [16]. This condition is found to hold for our data in the entire measurement range presented in Fig. 3(a). We also note that in a quasi-2D system, the parallel field may introduce a localization correction via the nonvanishing orbital motion along the z direction. Past studies on such 2 u.c. samples have shown that the orbital effects of the parallel fields are insignificant in comparison to the observed magnetoresistance features in our system [8].

As the NTO thickness is increased, a negative component in the MR emerges and eventually dominates the sample behavior in the parallel magnetic field [Figs. 3(b)–3(d)]. The large negative MR observed under $B_\parallel$ for the 10 and 20 u.c. samples cannot be explained by the WAL/WL effect. It is well known that the Kondo effect can play an important role in STO-based complex oxide systems, leading to negative MR [12,19]. The specific expression for the Kondo resistance as a function of the applied magnetic field has been derived by the Bethe-ansatz approach for zero temperature and is a universal function of B in units of a magnetic scale B_K [12,20]. The expression of the Kondo contribution to the MR for the case of parallel magnetic field $B_\parallel$ is given by

$$\frac{R(B_\parallel)-R(0)}{R(0)} = -\frac{R_K(0)}{R(0)}\left(1-\cos^2\left[\frac{\pi}{2}M^i(B_\parallel/B_K)\right]\right), \quad (5)$$

where $R(0)$ and $R_K(0)$ are the zero-field values of the total sample resistance and that of the Kondo contribution, respectively (see Appendix A for the exact form of the function M^i). The negative MR changes quadratically with $B_\parallel$ for $B_\parallel \ll B_K$ and decreases more gradually for $B_\parallel \gg B_K$.

To incorporate the effect of local magnetism into the Kondo model, we adopt a similar approach as described above by introducing the exchange field $B_\parallel^E$. As a result, the applied field $B_\parallel$ in Eq. (5) is replaced by a total effective field in the plane $B_\parallel + B_\parallel^E$, where the $B_\parallel$ dependence of $B_\parallel^E$ is given by the Langevin function. Using B_K, $\lambda\mu_0 M_s$, and μ_m as fit variables, the negative MR data observed in the 10 and 20 u.c. samples are well reproduced by this model. The fits are shown in Figs. 3(c) and 3(d) for various temperatures. We note that the zero-field value of $R_K(0)/R(0)$ in Eq. (5) is obtained for each temperature from the R vs T fit of the same sample [Figs. 2(c) and 2(d)] and is not a free parameter.

Figure 3(e) shows the extracted values of the Kondo magnetic scale B_K as a function of temperature for the 10 and 20 u.c. samples. B_K decreases monotonically with decreasing temperature. As the temperature is reduced below ~10 K, the extracted B_K values for the two samples saturate around a low-temperature limit between ~20 and 25 T. This saturation is expected as Eq. (5) is derived for $T \ll T_K$. The two distinct Kondo scales T_K and B_K are related. Assuming $g = 2$, the ratio of $k_B T_K$ to $g\mu_B B_K$ is found to be of order one, in agreement with the prediction of the spin-$\frac{1}{2}$ Kondo model [21].

In the above analyses, we focus on the limit cases where either the WAL or the Kondo effect dominate the in-plane MR. The 4 u.c. sample illustrates the crossover regime, where both positive and negative MR can be seen [Fig. 3(b)]. In this intermediate case, both the WAL and Kondo effects and their interplay are expected to play significant roles in the magnetotransport. Since the exact interplay between WAL and Kondo channels is not presently known, fitting of this complex crossover was not possible. In particular, assuming that the two channels are independent does not yield satisfactory fits.

Our analysis of the magneotresistance under parallel field provides a quantitative assessment of the magnetic moments of individual local magnetic regions at the interfaces. The extracted values of μ_m for all the four samples are shown in Fig. 3(f). The inverse of the apparent moment $1/\mu_m$ changes linearly with the inverse of the temperature. This behavior is consistent with the scenario of weakly interacting superparamagnets. The true moment μ_m^* is given by the relation $1/\mu_m = 1/\mu_m^*(1 + T^*/T)$, where T^* characterizes the energy scale of the dipole-diple interaction [22]. Fitting to this expression, we obtain the average magnetic moment of an individual nanoscale magnetic region to be $\mu_m^* = 22 \pm 1$, 12 ± 2, and $15 \pm 2\,\mu_B$ for the 2, 10, and 20 u.c. samples, respectively.

We now discuss possible microscopic origins of the coexistence of the Kondo impurities with local magnetic order revealed in this study. The ferromagnetic order in STO/NTO interfaces is thought to originate from the canting of the antiferromagnetic moments on the Ti^{3+} sublattice in NTO, likely mediated by Dzyaloshinskii-Moriya (DM) interaction [7,9], and can give rise to nanoscale superparamagnetic regions due to factors such as local strain [7]. Moreover, in STO/NTO/STO heterostructures, electron transfer between the STO and NTO layers can change a small density of Ti^{4+} in STO into the 3+ valence state [5]. These sparse Ti^{3+} moments in the STO layer can act as Kondo scattering centers at the conductive bottom interface. For thicker NTO layers, the Ti^{3+} fraction in the bottom STO is expected to increase [5]. Moreover, trace concentrations of oxygen vacancies and intermixed cations could also act as possible Kondo impurities [23]. Although remaining below the detection limit of microscopy techniques, their concentrations could be enhanced during the growth of thicker NTO samples, as the samples are maintained at higher temperatures for longer periods of time, facilitating their formation and diffusion.

IV. CONCLUSION

In summary, we investigated the low-temperature magneto-transport in a series of STO/NTO/STO heterointerfaces with different thicknesses of the NTO layer. Our analysis shows that increasing the thickness of the NTO layer introduces substantial Kondo scattering at the interface, which dominates over WAL in the thickest samples studied. Interestingly, we find that the effects of the SOC and Kondo scattering are enhanced by the presence of

local magnetic order, leading to a distinct magnetoresistance behavior in a parallel magnetic field. This serves as a sensitive probe of the magnetic landscape requiring only electrical transport measurements, capable of detecting ensembles ranging from small magnetically ordered regions down to atomic-scale magnetic scattering sites. We expect that this approach is applicable not just to oxide interfaces, but also to other 2D conducting systems. The coexistence of Kondo scattering, nanoscale magnetically ordered regions, magnetic exchange, and spin-orbit coupling, which can be controlled, e.g., by varying the NTO layer thickness identify NTO/STO interfaces as a promising system for possible applications, such as oxide spintronics.

ACKNOWLEDGEMENTS

This work was supported primarily by the Office of Naval Research under Award No. N00014-17-1-2884. Film growth and structural characterizations were funded by the U.S. Department of Energy through the University of Minnesota Center for Quantum Materials, under Grant No. DE-SC-0016371. Portions of this work were conducted in the Minnesota Nano Center, which is supported by the National Science Foundation through the National Nano Coordinated Infrastructure Network (NNCI) under Award No. ECCS-2025124. Sample structural characterization was carried out at the University of Minnesota Characterization Facility, which receives partial support from NSF through the MRSEC program under Award No. DMR-2011401. The authors would like to thank Z. Jiang and X. Fu for assistance with PPMS measurements, and P. Crowell, Y. Ayino, X. Ying, and A. Gatto Lamas for valuable discussions.

APPENDIX A: ZERO-TEMPERATURE MAGNETIZATION OF THE SPIN-$\frac{1}{2}$ KONDO MODEL

To calculate the magnetoresistance contribution from the Kondo effect, we adopt the model obtained by the Bethe-ansatz approach [12,20]. For a Kondo impurity with a spin of $S = \frac{1}{2}$, the impurity magnetization curve at zero temperature has the form

$$M^i(B/B_K) = \begin{cases} \dfrac{1}{\sqrt{2\pi}} \displaystyle\sum_{k=0}^{\infty} \left(-\frac{1}{2}\right)^k (k!)^{-1} (k+1/2)^{k-1/2} e^{-(k+1/2)} \left[\frac{B}{B_K}\right]^{2k+1}, & B \leqslant \sqrt{2} B_K \\ 1 - \pi^{-3/2} \displaystyle\int_0^{\infty} \frac{dt}{t} \sin(\pi t) \left[\frac{B_K}{B}\right]^{2t} e^{-t \ln(t/2e)} \Gamma\left(\frac{1}{2} + t\right), & \sqrt{2} B_K \leqslant B \end{cases} \tag{A1}$$

which is a universal function of the applied magnetic field B in units of B_K. B_K is a magnetic scale related to the Kondo temperature. We use this standard form in Eq. (5) of the main text for the theoretical fitting.

APPENDIX B: MAGNETORESISTANCE IN A PERPENDICULAR MAGNETIC FIELD

Here, we discuss the sample magnetoresistance (MR) measured under perpendicular magnetic field $B_\perp$ and the fittings of the theoretical models for the low-field regime.

As can be seen in Fig. 4(a), the MR vs $B_\perp$ curves of the 2 u.c. sample have the characteristic shapes of the weak antilocalization (WAL). The WAL is a manifestation of the spin-orbit coupling (SOC) in a diffusive electron system. Previous analysis of the WAL data using the Iordanskii, Lyanda-Geller, and Pikus (ILP) theory reveals that the dominant form of SOC in a 2 u.c. sample is likely cubic Rashba [8]. The lack of spatial inversion symmetry in the interface leads to a spin splitting of electron spectra called the Rashba effect. Unlike the typical k-linear Rashba in many systems, where the spin splitting is proportional to the wave vector k, in our interface the splitting has a dominant term cubic in k. The k-cubic dependence of the splitting is possibly associated with the orbital ordering of the d-electron subbands in $SrTiO_3$ [24,25].

The expression of the ILP model with the k-cubic spin splitting has the form [26,27]

$$\frac{R_s(B_\perp) - R_s(0)}{R_s(0)^2} = \sigma_0 \left[\frac{1}{2} \Psi\left(\frac{1}{2} + \frac{B_1}{B_\perp}\right) - \Psi\left(\frac{1}{2} + \frac{B_1 + B_2}{B_\perp}\right) - \frac{1}{2} \Psi\left(\frac{1}{2} + \frac{B_1 + 2B_2}{B_\perp}\right) - \frac{1}{2} \ln\left(\frac{B_1}{B_\perp}\right) + \ln\left(\frac{B_1 + B_2}{B_\perp}\right) + \frac{1}{2} \ln\left(\frac{B_1 + 2B_2}{B_\perp}\right) \right], \tag{B1}$$

Ψ is the digamma function. $B_{1,2}$ are the effective fields associated with inelastic scattering, SOC, and magnetic impurity scattering. In the absence of magnetic impurites, B_1 and B_2 directly correspond to the dephasing and SOC parameters, that is $B_1 = B_\phi$ and $B_2 = B_{so}$.

In Fig. 4(a) for the 2 u.c. sample, the solid lines show the best fits obtained using Eq. (B1) with B_1 and B_2 as the fit parameters. The data are well reproduced by the model. The extracted values of B_1 and B_2 are plotted as a function of temperature in the right panel of Fig. 4(a). It is important to note that in the 2 u.c. sample, the effect of magnetic impurities is negligible (see main text). Thus, the extracted values of B_1 and B_2 can be used directly for B_ϕ and B_{so}. In the main text, we substitute these values of B_ϕ and B_{so} in Eqs. (3)

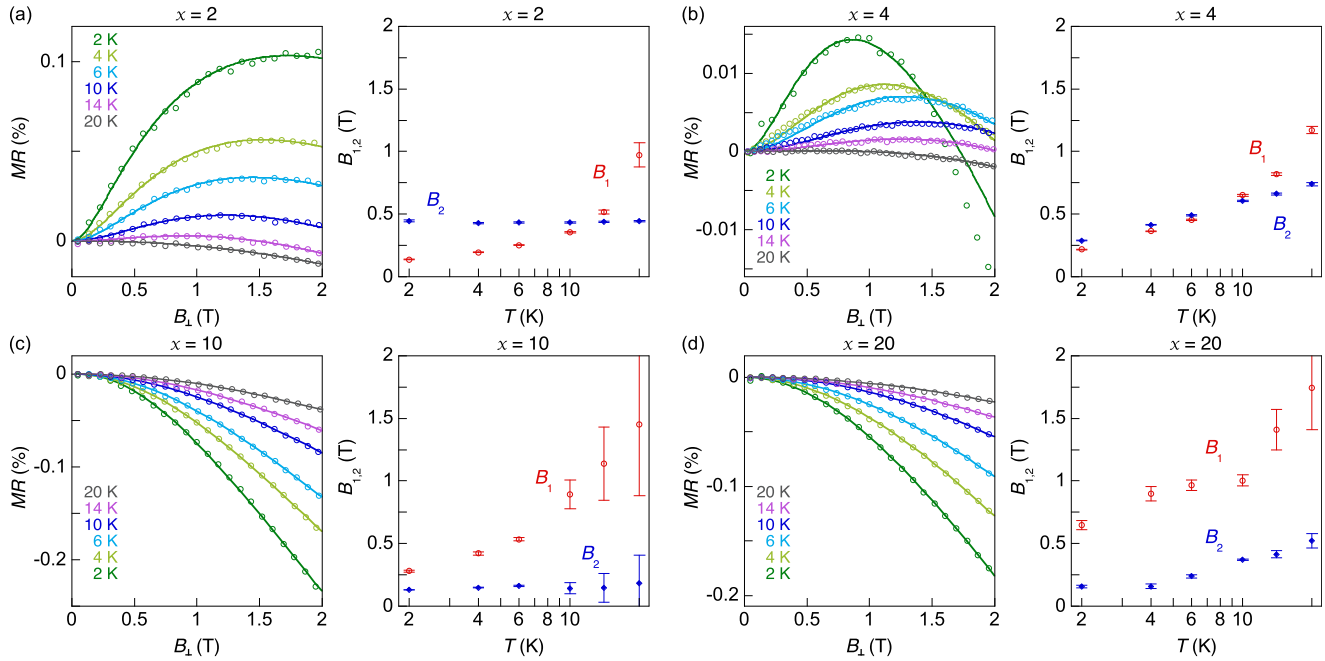

FIG. 4. Magnetoresistance as a function of the perpendicular magnetic field $B_\perp$ at various temperatures for samples with different NTO thicknesses, $x = 2$ (a), 4 (b), 10 (c), 20 u.c. (d): experimental data (open circles) and theoretical fits (solid lines). The extracted values of the fit parameters B_1 and B_2 are plotted as a function of temperature for each sample. The vertical bars represent the standard errors of the data points obtained from the fittings.

and (4) for the fittings of the in-plane field data of the same sample.

The results for the 4 u.c. sample are shown in Fig. 4(b). Again, we fit Eq. (B1) to the MR data at low $B_\perp$. The extracted values of $B_{1,2}$ are plotted in the right panel of Fig. 4(b). It should be noted that for this sample at $T = 2\,\mathrm{K}$, we find the WAL model can fit the experimental data well only up to around $B_\perp = 1.5\,\mathrm{T}$ [Fig. 4(b), left panel]. The deviation for $B_\perp > 1.5\,\mathrm{T}$ is likely due to the presence of the Kondo effect (see the main text). The Kondo effect contributes to a negative MR component whose overall amplitude increases with decreasing T.

For the theoretical fittings to the MR vs $B_\perp$ data of the 10 and 20 u.c samples, we take into account both the WAL/WL and the Kondo effect, by combining the existing models

$$\frac{\Delta R}{R} = \frac{\Delta R_{\mathrm{loc}} + \Delta R_K}{R} = -R_s(0)\sigma_0 F\left(\frac{B_1}{B_\perp}, \frac{B_2}{B_\perp}\right) - \frac{R_K(0)}{R(0)}\left\{1 - \cos^2\left[\frac{\pi}{2}M^i\left(\frac{B_\perp}{B_K}\right)\right]\right\}. \quad \text{(B2)}$$

The first term is the MR contribution from the WAL/WL, which has the form of Eq. (B1). The second term is the contribution from the Kondo effect. We adopt the same model as that used in the main text [Eq. (5)] by assuming that the Kondo scattering is isotropic. The exact form of the function M_i is given by Eq. (A1). $R_K(0)/R(0)$ is the ratio of the Kondo resistance to the total resistance at $B = 0$. Since we have obtained the values of $R_K(0)/R(0)$ and B_K from the R vs T and the MR vs $B_\parallel$ fits (see main text), the second term in Eq. (B2) can be calculated.

Figures 4(c) and 4(d) show the fitting results for the 10 and 20 u.c. samples, respectively. Due to the presence of magnetic impurities, the extracted values of $B_{1,2}$ are related to not only B_ϕ and B_{so} but also the magnetic scattering parameter B_s [14,28]. As B_1 is greater than B_2 for all the temperatures, the first term in Eq. (B2) gives rise to a negative MR component for all temperatures, which can be considered as the weak localization (WL). For perpendicular magnetic field, the WAL/WL is expected to play a significant role in the magnetotransport since the geometrical confinement for the orbital effects is absent. On the other hand, although we assume that the scattering from the Kondo impurities is isotropic, the Kondo contribution to MR is expected to be much weaker in $B_\perp$ than in $B_\parallel$. This is associated with the anisotropy of the exchange field from local magnetic order (see below).

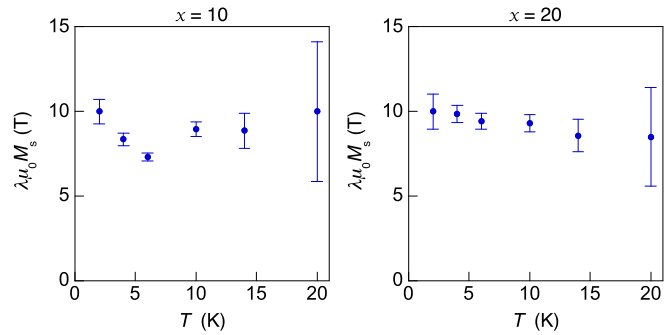

FIG. 5. The saturation exchange field $\lambda\mu_0 M_s$ as a function of temperature T, extracted from the fits in Figs. 3(c) and 3(d) for the 10 and 20 u.c. samples, respectively. Standard errors of the fits are included.

As expected for a thin magnetic film, the magnetization of local magnetic regions in the interface would have an easy-plane anisotropy. At small values of $B_\perp$, the magnetization would primarily lie in the sample plane. The out-of-plane component of the exchange field is negligible. However, at large enough values, an applied perpendicular field $B_\perp$ can overcome the in-plane anisotropy and pull the magnetization out of the plane. In this case, the exchange field would contribute substantially to the out-of-plane direction. A previous study of the angular dependence of the WAL effect for the 2 u.c. samples supports this scenario [8]. The critical value of $B_\perp$ to overcome the anisotropy was found between 2 and 2.5 T [8]. As a result, in order to avoid the complications arising from the local magnetic order, here, we fit to the MR vs $B_\perp$ data in the low-field regime, up to 2 T.

APPENDIX C: TEMPERATURE DEPENDENCE OF SATURATION EXCHANGE FIELD $\lambda\mu_0 M_s$

The saturation exchange field $\lambda\mu_0 M_s$ is expected to be weakly dependent on temperature. To improve the fit robustness, we restricted the values of $\lambda\mu_0 M_s$ to intervals of 5 T and analyzed the relative standard error in each interval to determine the best fit. The best fit occurred in the 5–10 T interval for both the 10 and the 20 u.c. samples, shown in Fig. 5.

[1] A. Ohtomo and H. Y. Hwang, Nature (London) **427**, 423 (2004).

[2] M. Takizawa, H. Wadati, K. Tanaka, M. Hashimoto, T. Yoshida, A. Fujimori, A. Chikamatsu, H. Kumigashira, M. Oshima, K. Shibuya, T. Mihara, T. Ohnishi, M. Lippmaa, M. Kawasaki, H. Koinuma, S. Okamoto, and A. J. Millis, Phys. Rev. Lett. **97**, 057601 (2006).

[3] P. Moetakef, T. A. Cain, D. G. Ouellette, J. Y. Zhang, D. O. Klenov, A. Janotti, C. G. Van de Walle, S. Rajan, S. J. Allen, and S. Stemmer, Appl. Phys. Lett. **99**, 232116 (2011).

[4] P. Xu, D. Phelan, J. Seok Jeong, K. Andre Mkhoyan, and B. Jalan, Appl. Phys. Lett. **104**, 082109 (2014).

[5] P. Xu, T. C. Droubay, J. S. Jeong, K. A. Mkhoyan, P. V. Sushko, S. A. Chambers, and B. Jalan, Adv. Mater. Interfaces **3**, 1500432 (2016).

[6] P. Xu, Y. Ayino, C. Cheng, V. S. Pribiag, R. B. Comes, P. V. Sushko, S. A. Chambers, and B. Jalan, Phys. Rev. Lett. **117**, 106803 (2016).

[7] Y. Ayino, P. Xu, J. Tigre-Lazo, J. Yue, B. Jalan, and V. S. Pribiag, Phys. Rev. Mater. **2**, 031401(R) (2018).

[8] X. Cai, Y. Ayino, J. Yue, P. Xu, B. Jalan, and V. S. Pribiag, Phys. Rev. B **100**, 081402(R) (2019).

[9] A. S. Sefat, J. E. Greedan, G. M. Luke, M. Niéwczas, J. D. Garrett, H. Dabkowska, and A. Dabkowski, Phys. Rev. B **74**, 104419 (2006).

[10] G. Amow and J. Greedan, J. Solid State Chem. **121**, 443 (1996).

[11] A. S. Sefat, J. E. Greedan, and L. Cranswick, Phys. Rev. B **74**, 104418 (2006).

[12] M. Lee, J. R. Williams, S. Zhang, C. D. Frisbie, and D. Goldhaber-Gordon, Phys. Rev. Lett. **107**, 256601 (2011).

[13] T. A. Costi, A. C. Hewson, and V. Zlatic, J. Phys.: Condens. Matter **6**, 2519 (1994).

[14] V. V. Bal, Z. Huang, K. Han, Ariando, T. Venkatesan, and V. Chandrasekhar, Phys. Rev. B **99**, 035408 (2019).

[15] G. M. Minkov, A. V. Germanenko, O. E. Rut, A. A. Sherstobitov, L. E. Golub, B. N. Zvonkov, and M. Willander, Phys. Rev. B **70**, 155323 (2004).

[16] A. G. Mal'shukov, K. A. Chao, and M. Willander, Phys. Rev. B **56**, 6436 (1997).

[17] V. K. Dugaev, P. Bruno, and J. Barnas, Phys. Rev. B **64**, 144423 (2001).

[18] R. C. O'Handley, *Modern Magnetic Materials: Principles and Applications* (Wiley, Hoboken, NJ, 2000).

[19] A. Joshua, J. Ruhman, S. Pecker, E. Altman, and S. Ilani, Proc. Natl. Acad. Sci. USA **110**, 9633 (2013).

[20] N. Andrei, K. Furuya, and J. H. Lowenstein, Rev. Mod. Phys. **55**, 331 (1983).

[21] K. Furuya and J. H. Lowenstein, Phys. Rev. B **25**, 5935 (1982).

[22] P. Allia, M. Coisson, P. Tiberto, F. Vinai, M. Knobel, M. A. Novak, and W. C. Nunes, Phys. Rev. B **64**, 144420 (2001).

[23] N. Pavlenko, T. Kopp, E. Y. Tsymbal, J. Mannhart, and G. A. Sawatzky, Phys. Rev. B **86**, 064431 (2012).

[24] P. D. C. King, S. McKeown Walker, A. Tamai, A. de la Torre, T. Eknapakul, P. Buaphet, S.-K. Mo, W. Meevasana, M. S. Bahramy, and F. Baumberger, Nat. Commun. **5**, 3414 (2014).

[25] H. Nakamura, T. Koga, and T. Kimura, Phys. Rev. Lett. **108**, 206601 (2012).

[26] S. V. Iordanskii, Yu. B. Lyanda-Geller, and G. E. Pikus, Pis'ma Zh. Eksp. Teor. Fiz. **60**, 199 (1994) [JETP Lett. **60**, 206 (1994)].

[27] W. Knap, C. Skierbiszewski, A. Zduniak, E. Litwin-Staszewska, D. Bertho, F. Kobbi, J. L. Robert, G. E. Pikus, F. G. Pikus, S. V. Iordanskii, V. Mosser, K. Zekentes, and Y. B. Lyanda-Geller, Phys. Rev. B **53**, 3912 (1996).

[28] S. Hikami, A. I. Larkin, and Y. Nagaoka, Prog. Theor. Phys. **63**, 707 (1980).